

Fatigue strength of 30XГСА–40ХМФА welded joints produced by rotary friction welding

© 2023

*Elena Yu. Priymak**^{1,2,4}, PhD (Engineering), Head of the Laboratory of Metal Science and Heat Treatment, assistant professor of Chair of Materials Science and Technology of Materials

*Elena A. Kuzmina*¹, Head of Technical Department

Sergey V. Gladkovskii^{3,5}, Doctor of Sciences (Engineering), chief researcher

Dmitry I. Vichuzhanin^{3,6}, PhD (Engineering), senior researcher

Valeria E. Veselova^{3,7}, junior researcher

¹ZBO Drill Industries, Inc., Orenburg (Russia)

²Orenburg State University, Orenburg (Russia)

³Institute of Engineering Science of Ural Branch of the Russian Academy of Sciences, Yekaterinburg (Russia)

*E-mail: elena-pijmak@yandex.ru

⁴ORCID: <https://orcid.org/0000-0002-4571-2410>

⁵ORCID: <https://orcid.org/0000-0002-3542-6242>

⁶ORCID: <https://orcid.org/0000-0002-6508-6859>

⁷ORCID: <https://orcid.org/0000-0002-4955-6435>

Received 02.11.2022

Accepted 16.02.2023

Abstract: Rotary friction welding (RFW) is used in the production of drill pipes for solid mineral prospecting. The need for the creation of the lightened drill strings for high-speed diamond drilling of ultradeep wells dictates the necessity of a greater focus on the study of a weld zone and setting the RFW technological parameters. This paper presents the results of experimental studies of a welded joint of a drill pipe of the H standard size according to ISO 10097, made of the 30XГСА (pipe body) and 40ХМФА (tool joint) steels under the cyclic loads. The authors evaluated the influence of the force applied to the workpieces in the process of friction of the contacting surfaces (force during heating), and postweld tempering at a temperature of 550 °C on the cyclic life of welded joints, under the conditions of alternate tension-compression at the cycle amplitude stress of ± 420 MPa. The study determined that with an increase in the force during heating, the microstructure changes occur in the zone of thermomechanical influence, contributing to an increase in the fatigue strength of welded joints. The authors identified the negative effect of postweld tempering on the fatigue strength of welded joints, which is expressed in the decrease in the number of cycles before failure by 15–40 %, depending on the magnitude of the force during heating. The optimal RFW mode of the specified combination of steels is determined, which provides the largest number of cycles before failure: the force during heating (at friction) $F_h=120$ kN, forging force $F_{for}=160$ kN, rotational frequency during heating $n=800$ Rpm, and upset during heating $l=8$ mm. A series of fatigue tests have been carried out at various values of the cycle amplitude stress of the welded joint produced at the optimal mode and the 30XГСА steel base metal; limited endurance curves have been plotted. It is shown that the differences in the limited endurance curves of the pipe body material (30XГСА steel) and the welded joint are insignificant. The obtained results are supplemented by the microhardness measurement data and fractographs of fractured samples, revealing the mechanism of crack propagation under the cyclic loads.

Keywords: rotary friction welding; drill pipes; welded joint; fatigue strength; limited endurance curve; 30XГСА steel; 40ХМФА steel.

Acknowledgments: The reported study was funded by RFBR according to the research project No. 20-38-90032.

To perform mechanical tests, the equipment of the “Plastometry” Core Facility Center of Institute of Engineering Science of the UB RAS was used.

For citation: Priymak E.Yu., Kuzmina E.A., Gladkovskii S.V., Vichuzhanin D.I., Veselova V.E. Fatigue strength of 30XГСА–40ХМФА welded joints produced by rotary friction welding. *Frontier Materials & Technologies*, 2023, no. 1, pp. 69–81. DOI: 10.18323/2782-4039-2023-1-69-81.

INTRODUCTION

Rotary friction welding (RFW) refers to the process of producing welded joints of parts that are rotary bodies. It has a number of technological advantages compared to other types of welding and allows welding partially weldable and difficult-to-weld materials in various combinations, which determines its application in various industries. This technology is used when producing drill pipes with welded tool joints for the oil and mining industry, during geological

exploration for solid minerals. At the same time, the exaggeration of mining and geological drilling conditions associated with a greater depth of rock occurrence, determines the necessity to create lightened drill pipe structures by reducing the wall thickness of the drill pipe body when using a stronger pipe billet. Considering that the drill string during high-speed diamond drilling operates under difficult mechanical loading conditions, a more careful approach is required to the choice of materials and the setting of welding modes.

As a rule, drill pipes are a welded structure of a tool joint with a pipe body made of medium- and low-carbon alloy steels connected by RFW¹. As a pipe body for lightened constructions of drill pipes, it is supposed to use a pipe billet made of 30XГCA steel, which after quenching and tempering, ensures the required properties: constrained yield strength ≥ 750 MPa, ultimate tensile strength ≥ 850 MPa, and elongation ≥ 12 %. As a material for the drill pipe tool joint, various grades of medium-carbon alloy steels can be used, which after quenching and tempering, ensure the following mechanical properties: constrained yield strength ≥ 930 MPa, ultimate tensile strength ≥ 1050 MPa, and relative elongation ≥ 10 %. 40XMΦA steel is the most widely used.

The search and analysis of works aimed at the detailed study of the microstructure and properties of friction welded joints made of medium-carbon alloy steels showed the insufficient information in this area. There are some publications presenting the results of the studies of the microstructure and properties of welded joints of drill pipes made of N80 steels (analogue to 35Г2) in the normalized state with 42CrMo4 steel (analogue to 40XM) after quenching and tempering [1], AISI 8630 steel (analogue to 30XMH) [2], and welded joints of ASTM A 106 Grade B steel (analogue to 20Г) in the hot-rolled state and 4140 steel (analogue to 40XГM) after normalization and after toughening [3; 4]. These works, as well as other studies [5; 6] indicate that the mechanical properties of welded joints during tensile tests with properly selected welding modes meet or, in some cases, even exceed the mechanical properties of the weakest welded material. However, the working conditions of drill pipes during operation are determined by the impact of both the static and sign-variable cyclic loads. Therefore, the study of the fatigue strength of the RFW-produced joints of drill pipe elements is important to assess the reliability and performance of the structure.

It is known that the fatigue properties of welded joints, including those RFW-produced, are determined both by the chemical composition of welded materials and the microstructural features of the welded joint zone and the level of residual welding stresses [7; 8]. In this case, welded joints performed by the friction welding methods have higher fatigue strength characteristics than welded joints produced by fusion welding [9–11]. In the work [12], it was established that a higher endurance limit of a welded joint compared to the base material can be obtained by friction welding of stainless steels. However, when welding dissimilar steels, such as medium-carbon steel and austenitic stainless steel, the fatigue strength of a welded joint decreased by 30 % compared to medium-carbon steel and by 40 % compared to austenitic steel [13]. During friction welding of AISI 1040 medium-carbon steel (analogue to 40Г), the fatigue strength of a welded joint is close to the fatigue strength of the base metal of this steel [14]. However, the fatigue strength of a welded joint in the combination of 32G2 and 40HN steels is inferior to the fatigue strength of 32G2 steel by up to 30 % [15].

At the same time, welding parameters and post-weld heat treatment affect the microstructure and properties of welded joints, which is shown in publications using the examples of both the joints of medium-carbon steels [16; 17] and combinations of low-carbon steel with stainless steel [18] and aluminium alloy [19], as well as other alloys [20] and their combinations [21].

The need to create lightened structures of geological exploration drill pipes dictates the necessity to study the fatigue properties when changing the modes of welding and post-weld heat treatment also in a welded joint of 30XГCA and 40XMΦA steels intended for use, which has not been studied by now. It is necessary to understand the degree of strength uniformity of the weld zone with the drill pipe body (30XГCA steel).

Early studies of mentioned combination of steels identified the optimal range of RFW parameters, which provides maximum tensile strength at their interface (at the joint): heating force $F_h=40\text{--}120$ kN, forging force $F_{\text{for}}=100\text{--}160$ kN, rotational speed during heating $n=700\text{--}900$ Rpm, and upset during heating $l=-7\text{--}9$ mm [22]. However, the obtained values of optimal parameters show that the range of force values during heating ensuring a high-quality welded joint in the junction of materials, is rather wide, therefore, a more detailed assessment of the influence of this parameter on the fatigue strength of a joint containing all microstructural zones formed during welding is of interest.

The work is aimed at evaluating the influence of the parameters of rotary friction welding and post-weld tempering on the fatigue resistance of welded joints of 30XГCA and 40XMΦA steels, and determining the optimal parameters ensuring the maximum degree of strength uniformity of the weld zone with the base material – 30XГCA steel.

METHODS

Friction welding was performed on pipe billets with a diameter of 92 mm and a wall thickness of 8 mm made of 40XMΦA steel and pipe billets with a diameter of 89 mm and a wall thickness of 4 mm (H standard size according to ISO 10097) made of 30XГCA steel previously quenched and high-tempered.

Chemical composition of the original steels is shown in Table 1.

Welding was carried out on the Thompson-60 equipment complete with a software package that allows setting and controlling welding parameters. The RFW process consists of the stage of heating the billets during friction as a result of applying an axial force on the side of the rotating workpiece, and the forging stage, which consists of applying an additional axial force after the rotation stops. Thus, the main RFW parameters are the force during heating, (during friction as a result of the contact of two rotating pipes), F_h (kN), the forging force F_{for} (kN), the rotational speed during heating n (Rpm), and the upset during heating l (mm) [23].

Welding modes selected for current study are shown in Table 2.

The mechanical properties of welded joints and the base metal are shown in Table 3. It also contains the mechanical properties of welded joints after tempering in a laboratory furnace at a temperature of 550 °C during 1 hour.

¹ГОСТ P 51245–99. General-purpose steel drill pipes. General technical specifications. M.: Publishing House of Standards, 1999. 15 p.

Fatigue tests of the samples were carried out on the INSTRON 8801 universal testing machine according to the alternate tension-compression scheme with a cycle asymmetry coefficient $R=-1$, and a loading frequency of 5 Hz. The standard size of samples for fatigue tests of the base metal and welded joints is shown in Fig. 1. In this case, the sample shape corresponded to type III according to the ГОСТ 25.509-79 standards and the dimensions were adjusted to ensure its stability under alternating cyclic loading at the increased loads.

In the course of testing the samples of welded joints produced under various welding modes, in the initial state and after tempering, the number of cycles to failure was determined at a stress amplitude of $\sigma_a=\pm 420$ MPa. Three samples per mode were subjected to tests followed by the calculation of the average value of cyclic durability. After determining the optimal mode that ensures the maximum durability of welded specimens. Tests were carried out at various stresses both for welded specimens under the selected mode, and monolithic specimens made of 30XГСА steel for the construction of limited endurance curves and their comparative evaluation.

The study of the microstructure of welded joints was carried out on transverse microslices after etching with a 4 % solution of nitric acid in ethanol using an Olympus DSX1000 optical microscope. The microhardness was measured along the length of the thermomechanical effect zone (TMEZ), with a step of 0.5 mm according to the ГОСТ 9450-76 standard on a HVS-1000 microhardness tester, applying a load of 2 N for 10 s. The fractographic analysis of the destroyed samples was carried out on a Tescan VEGA II XMU scanning electron microscope.

RESULTS

A typical macro- and microstructure of a welded joint of 30XГСА and 40XMΦА steels after rotary friction welding is shown in Fig. 2. Directly near the joint zone, it is martensite with the bainite areas. In the TMEZ peripheral areas, a finely-dispersed ferrite-carbide microstructure is observed as a result of a decrease in temperature exposure.

Microhardness distribution across the width of TMEZ in the initial state after welding and tempering is shown in Fig. 3.

Near the zone of joining two steels, there are areas with high microhardness in relation to the base metal caused by the formation of martensite structures (Fig. 3 a). The force during heating has some influence both on the microhardness values and the TMEZ length. With an increase in the force during heating in the range from 40 kN (mode No. 1) to 120 kN (mode No. 3), the TMEZ length decreases from 7.85 to 5.25 mm. The maximum values of microhardness are observed in the samples obtained with a heating force of 120 kN and amount 669 HV 0.2 for 40XMΦА steel and 608 HV 0.2 for 30XГСА steel. The minimum HV 0.2 values correspond to the peripheral TMEZ areas in the welded joint produced with the lowest force during heating of 40 kN. In these areas, the microhardness of 30XГСА steel is 264–280 HV 0.2, the one of 40XMΦА steel is 298–335 HV 0.2, while the microhardness of the base metal of 30XГСА steel reaches 294–306 HV 0.2, and the one of 40XMΦА steel is 362–367 HV 0.2. Thus, the most weakened zone in this welded joint (mode No. 1) in relation to all its areas, is the peripheral area of the 30XГСА steel TMEZ.

Table 1. Chemical composition of steels intended for the production of drill pipes, % by weight
Таблица 1. Химический состав сталей, предназначенных для производства буровых труб, % по масс.

| Steel Grade | C | Mn | Si | S | P | Cr | Ni | Cu | Mo | V |
|----------------------|------|------|------|-------|-------|------|------|------|------|------|
| 30XГСА pipe body | 0.33 | 1.02 | 1.12 | 0.003 | 0.011 | 0.99 | – | 0.04 | – | – |
| 40XMΦА tool joint | 0.41 | 0.48 | 0.27 | 0.004 | 0.008 | 0.97 | 0.08 | 0.06 | 0.27 | 0.11 |

Table 2. Rotary friction welding modes selected for the experiment
Таблица 2. Режимы ротационной сварки трением, выбранные для эксперимента

| Mode No. | Force during heating F_h , kN | Forging force F_{for} , kN | Upset during heating l , mm | Rotational speed n , Rpm |
|----------|------------------------------------|---------------------------------|----------------------------------|-------------------------------|
| 1 | 40 | 160 | 8 | 800 |
| 2 | 80 | | | |
| 3 | 120 | | | |

Table 3. Mechanical properties of the RFW-produced welded joints of the 30XГСА and 40ХМФА steels and base materials*
Таблица 3. Механические свойства сварных соединений сталей 30XГСА и 40ХМФА, выполненных ротационной сваркой трением, и материалов основы*

| Test sample | RFW mode No. | $\sigma_{0,2}$, МПа | σ_B , МПа | δ , % | ψ , % |
|--------------|--------------|----------------------|------------------|--------------|------------|
| Welded joint | 1 | 760/758** | 849/841 | 8.0/7.0 | 34.5/33.5 |
| | 2 | 757/755 | 883/851 | 10.0/9.0 | 33.0/33.5 |
| | 3 | 771/768 | 894/882 | 10.5/10.5 | 35.0/36.0 |
| 30XГСА | – | 767 | 888 | 13.0 | 36.5 |
| 40ХМФА | – | 1111 | 1205 | 10.5 | 38.0 |

* Mechanical properties are obtained for the samples with the working part length of 50 mm, width of 15 mm, and thickness of 4 mm at the INSTRON 8801 test unit according to the GOST 6996-66 and GOST 1497-84 standards.

** In the numerator, mechanical properties of a welded joint after rotary friction welding are indicated; in the denominator – the ones after tempering.

* Механические свойства получены на образцах с длиной рабочей части 50 мм, шириной 15 мм и толщиной 4 мм на испытательной установке INSTRON 8801 в соответствии с ГОСТ 6996-66 и ГОСТ 1497-84.

** В числителе приведены механические свойства сварного соединения после ротационной сварки трением, а в знаменателе – после отпуска.

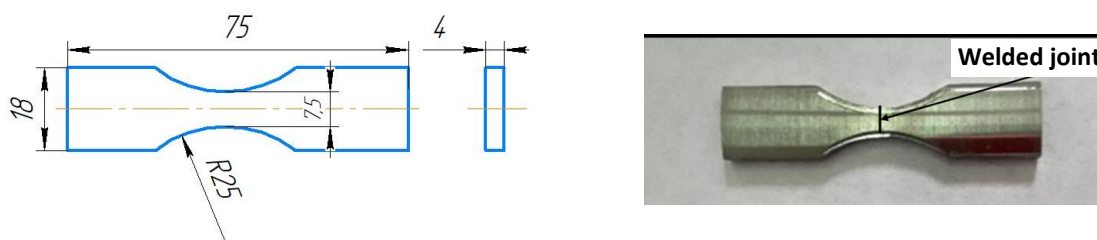


Fig. 1. A sample with a welded joint for fatigue tests
Рис. 1. Образец со сварным соединением для испытаний на усталость

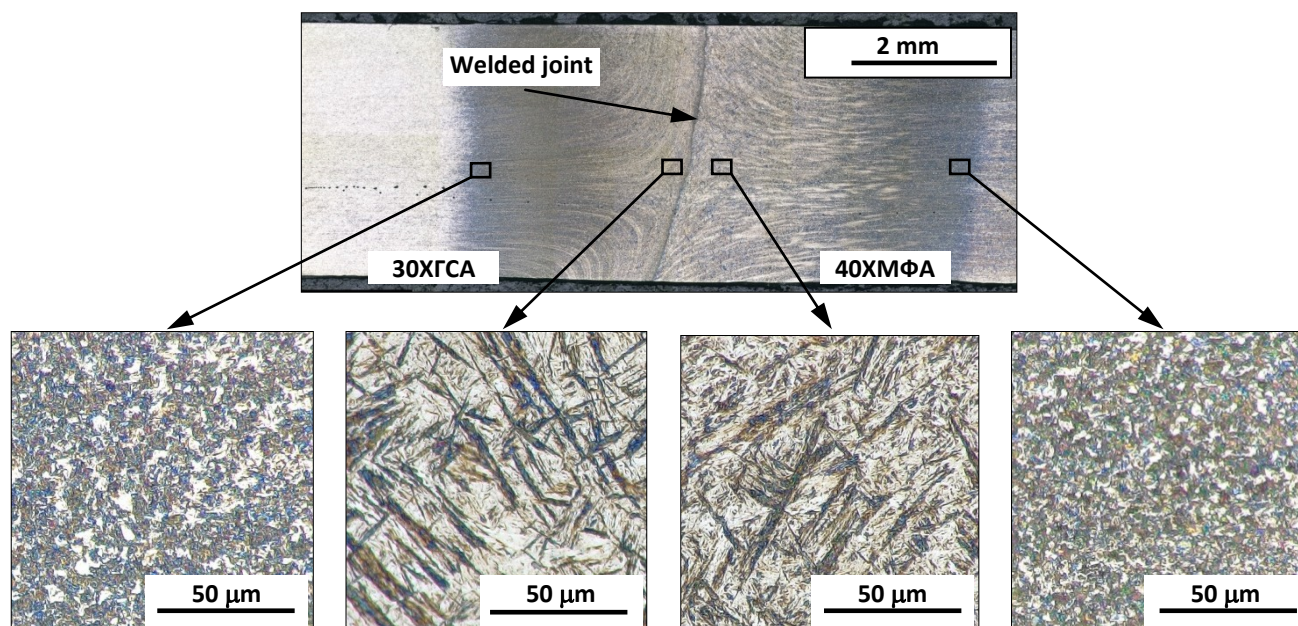


Fig. 2. Macro- and microstructure of a welded joint of the 30XГСА and 40ХМФА steels produced by rotary friction welding (mode No. 2)
Рис. 2. Макро- и микроструктура сварного соединения сталей 30XГСА и 40ХМФА, полученная ротационной сваркой трением (режим № 2)

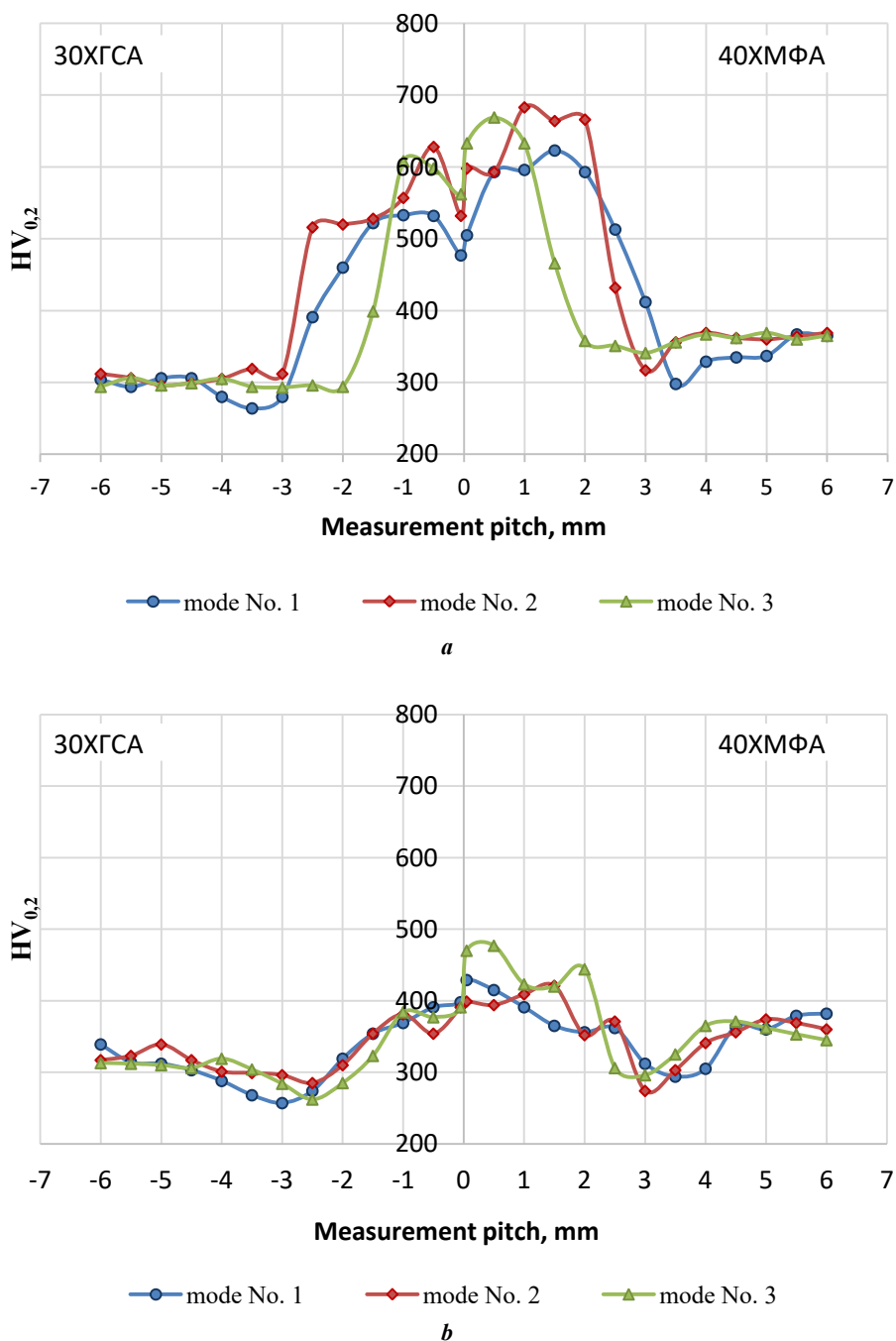


Fig. 3. Microhardness distribution in welded joints of the 30XГСА–40XМФА steels:
a – after friction welding; *b* – after friction welding and further tempering at 550 °C
Рис. 3. Распределение микротвердости в сварных соединениях сталей 30XГСА–40XМФА:
a – после сварки трением; *b* – после сварки трением и последующего отпуска при 550 °C

Post-weld tempering caused a decrease in microhardness in the thermomechanical effect zone in all samples and, as a result, a partial elimination of the mechanical inhomogeneity typical for the initial state of a welded joint. However, it should be noted that in the welded joints, performed according to modes No. 2 and No. 3, in the peripheral TMEZ areas, the microhardness in the initial state was at the base metal level, and local weakening of these areas with respect to the base metal is observed after tempering. In the welded joint, obtained according to mode No. 1, in the weakening zone formed earlier during

welding, an additional decrease in microhardness is observed (Fig. 3 b).

Fig. 4 shows the number of cycles before failure of samples of welded joints during fatigue testing.

The obtained results (Fig. 4) show that with an increase in the force during heating, the durability of the samples increases. At the same time, tempering reduces the number of cycles to failure by 40, 20, and 15 % after the implementation of modes No. 1, No. 2, and No. 3, respectively.

During the tests, the failure of all samples was recorded from the side of 30XГСА steel at a distance of 3 to 5 mm

from the junction of two steels. Fig. 5 shows the appearance of tested samples.

Fig. 6, 7 demonstrate the macro- and microstructure of fractures of tested samples.

The fracture surface of all tested samples is a typical fatigue fracture, where the zone of the fatigue crack initiation and development (area 1), as well as the fracture zone (area 2) are observed (Fig. 6 and 7). The fatigue zone in all samples of welded joints is from 65 to 75 %, which indicates a high resistance of the material to crack propagation. In this case, the fatigue crack initiation occurred from the surface of the samples on the inner part of the pipe billet.

The fatigue fracture zones of samples produced with the force during heating equal to 40 kN (mode No. 1) at $\sigma_a=420$ MPa with and without tempering have a plateau-like fracture surface with the fragments of a grooved microrelief (Fig. 6 b, 6 e). The tempered sample has a smoother microrelief (Fig. 6 e). However, the distance between the fatigue grooves is higher, which indicates

a higher crack propagation rate in this sample. The fracture zones of both samples (Fig. 6 c, 6 f) are of the viscous type and contain small and shallow viscous pits.

The fractures of samples of welded joints produced with the force during heating equal to 80 kN (mode No. 2) had an identical structure to that described above in the initial state and after tempering. However, samples obtained with the force during heating equal to 120 kN (mode No. 3), both with subsequent tempering (Fig. 7 e) and without it (Fig. 7 b), are characterized by a smoother microrelief without evident fatigue grooves. Taking into account the fact that the total TMEZ length at this welding mode is 5.25 mm, the failure of the sample, most likely, occurred in the zone of the base metal of 30XГСА steel (Fig. 5). In the fracture of the samples, pores are observed, which were probably initiated by the non-metallic inclusions in the original billet. The fracture zones of both samples (Fig. 7 c, 7 f), as well as in the previous samples, are characterized by the viscous shallow-pitted microrelief.

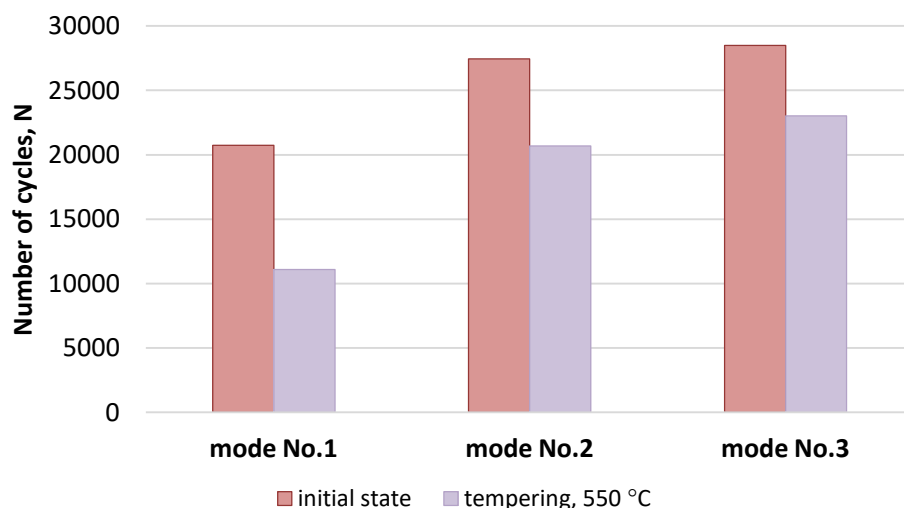


Fig. 4. The number of cycles before failure of samples of welded joints of the 30XГСА–40XMΦA steels in the initial state and after tempering during cyclic tests with an amplitude of $\sigma_a=\pm 420$ MPa

Рис. 4. Количество циклов до разрушения образцов сварных соединений сталей 30XГСА–40XMΦA в исходном состоянии и после отпуска при циклических испытаниях с амплитудой $\sigma_a=\pm 420$ МПа

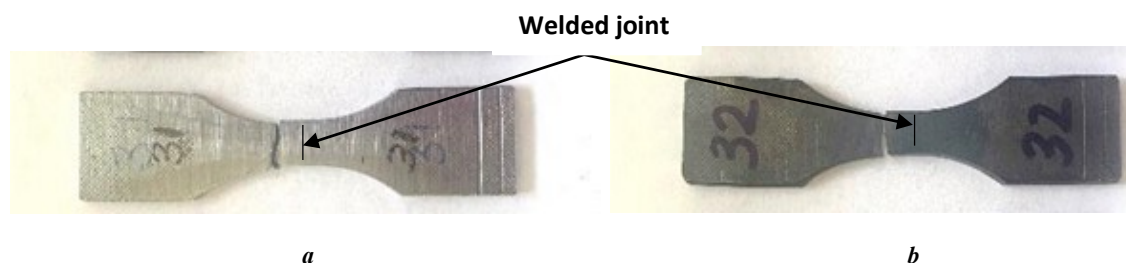


Fig. 5. The appearance of broken specimens after cyclic tests (at the left – 30XГСА steel):

a – mode No. 3 after welding; **b** – mode No. 3 after tempering

Рис. 5. Внешний вид разрушенных образцов после циклических испытаний (слева сталь 30XГСА):

a – режим № 3 после сварки; **b** – режим № 3 после отпуска

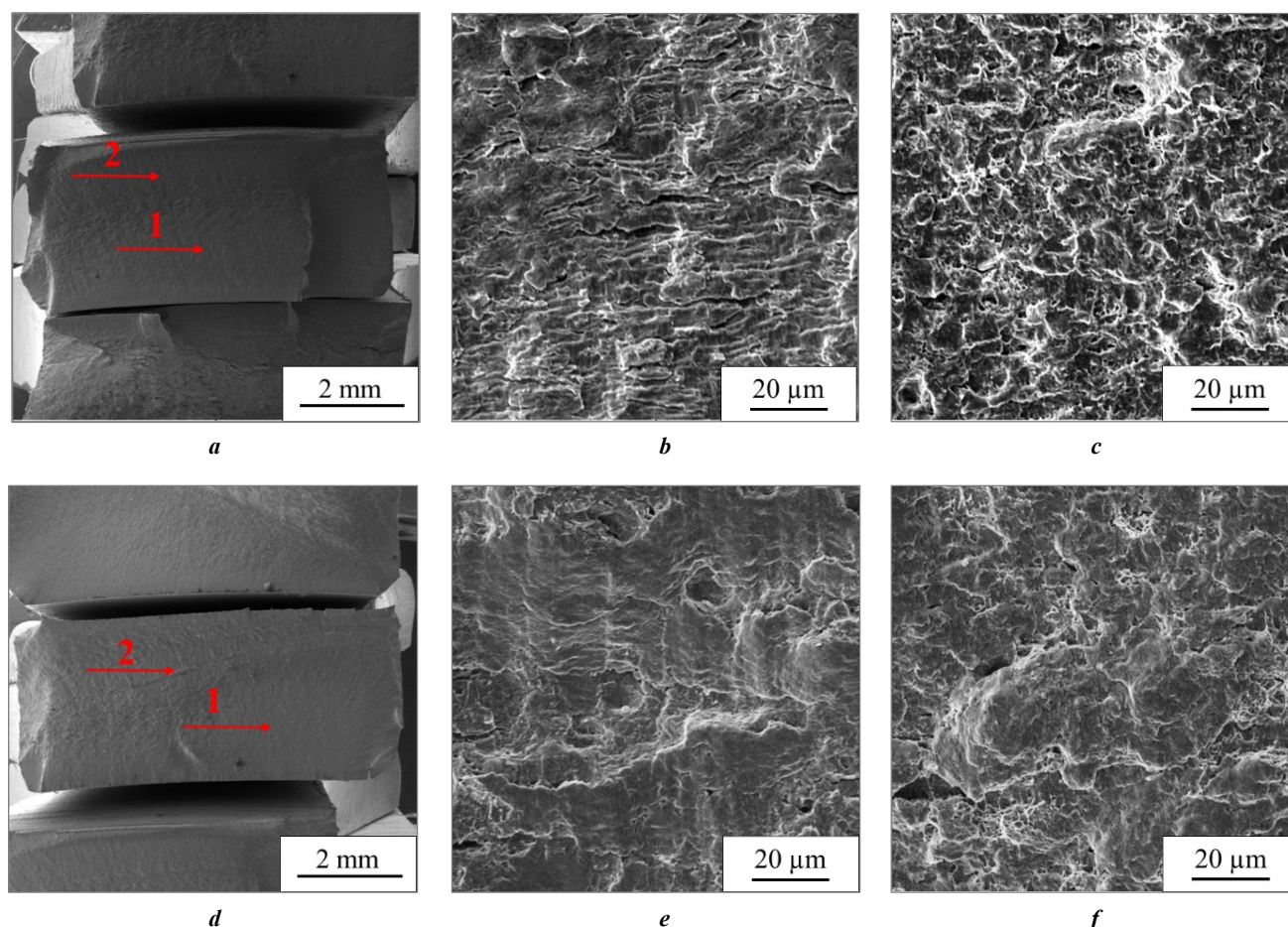


Fig. 6. Macro- (a, d) and microstructure (b, c, e, f) of fractures of welded joints after endurance tests after welding according to the mode No. 1 in the initial state (a–c, $\sigma_a=420$ MPa, $N=24142$) and after tempering (d–f, $\sigma_a=420$ MPa, $N=13631$): a, d – general appearance; b, e – area 1 (fatigue zone); c, f – area 2 (fracture zone)
Рис. 6. Макро- (a, d) и микростроение (b, c, e, f) изломов сварных соединений после испытаний на усталостную прочность после сварки по режиму № 1 в исходном состоянии (a–c, $\sigma_a=420$ МПа, $N=24142$) и после отпуска (d–f, $\sigma_a=420$ МПа, $N=13631$): a, d – общий вид; b, e – участок 1 (зона усталости); c, f – участок 2 (зона долома)

Thus, a welded joint produced with the force during heating $F_h=120$ kN (mode No. 3) without subsequent tempering has the highest fatigue strength among the investigated welding modes. Therefore, comparative tests of welded joints and the pipe body material for the construction of limited endurance curves were carried out in this mode. The curves in semilogarithmic coordinates obtained during testing are shown in Fig. 8.

The comparative evaluation of the limited endurance curves (Fig. 8) of this welded joint and the 30XГСА base steel shows that the differences are insignificant. In the low-cycle fatigue area ($N<1000$), the 30XГСА base steel has a bit higher fatigue resistance, while in the high-cycle fatigue area, the base steel and the welded joint have the same averaged level of the fatigue strength. A characteristic feature of the mechanical behaviour of welded joints under the cyclic loading conditions at all stress amplitudes is the destruction both in the zone of the initial material of 30XГСА steel and in the 30XГСА steel TMEZ, regardless of the σ_a value, which indicates the strength uniformity of these zones.

The morphology of the fracture surface of samples of welded joints and 30XГСА steel formed at different amplitude stresses is shown in Fig. 9, 10.

It is evident that at fracture in the stress range of ± 495 –508 MPa, there are some differences in the structure of fracture of welded joints and the 30XГСА steel base metal (Fig. 9). On the fatigue fracture surface of the welded joint specimen (Fig. 9 b), stepped plateau-like areas surrounded by dimples were formed. The fatigue grooves are indistinct. A rougher relief of the fatigue fracture zone is observed in the base metal specimen (Fig. 9 e). The crack initiation occurs in two areas of the sample, near the defects or inclusions (Fig. 9 d). The fracture zones of both samples (Fig. 9 c, 9 f) are characterized by the shallow-pitted microrelief.

With a decrease in the active stress and an increase in the number of cycles to failure, the plateau-like areas occupy the major area of the fatigue fracture zone (Fig. 10 a, 10 b, 10 d, 10 f). However, the fatigue grooves are clearly formed only in the small areas of fracture surfaces; in other areas, they are poorly formed and broken under the influence

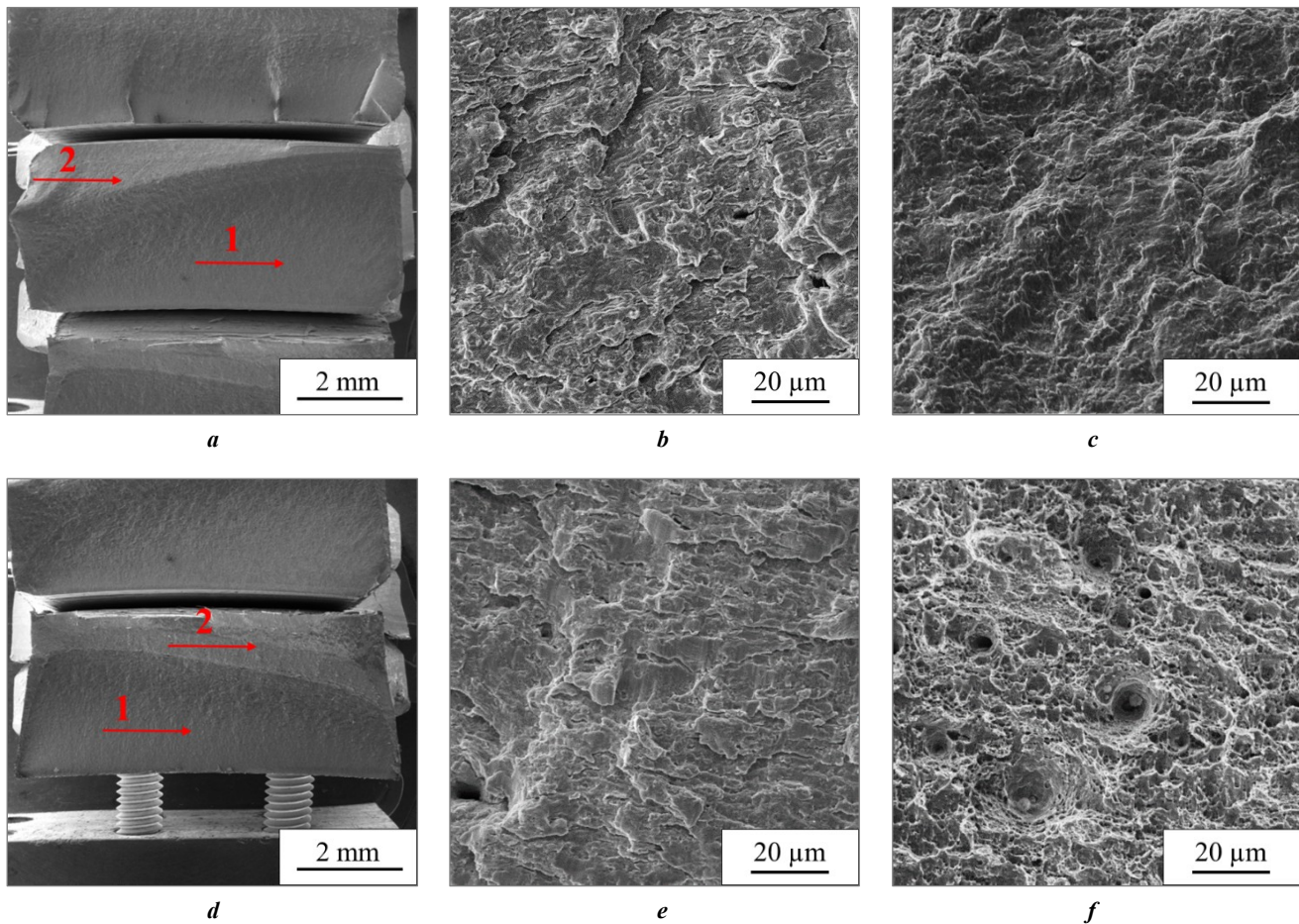


Fig. 7. Macro- (a, d) and microstructure (b, c, e, f) of fractures of welded joints after endurance tests after welding according to the mode No. 3 in the initial state (a–c, $\sigma_a=420$ MPa, $N=32825$) and after tempering (d–f, $\sigma_a=420$ MPa, $N=23384$): a, d – general appearance; b, e – area 1 (fatigue zone); c, f – area 2 (fracture zone)

Рис. 7. Макро- (a, d) и микростроение (b, c, e, f) изломов сварных соединений после испытаний на усталостную прочность после сварки по режиму № 3 в исходном состоянии (a–c, $\sigma_a=420$ МПа, $N=32825$) и после отпуски (d–f, $\sigma_a=420$ МПа, $N=23384$): a, d – общий вид; b, e – участок 1 (зона усталости); c, f – участок 2 (зона долома)

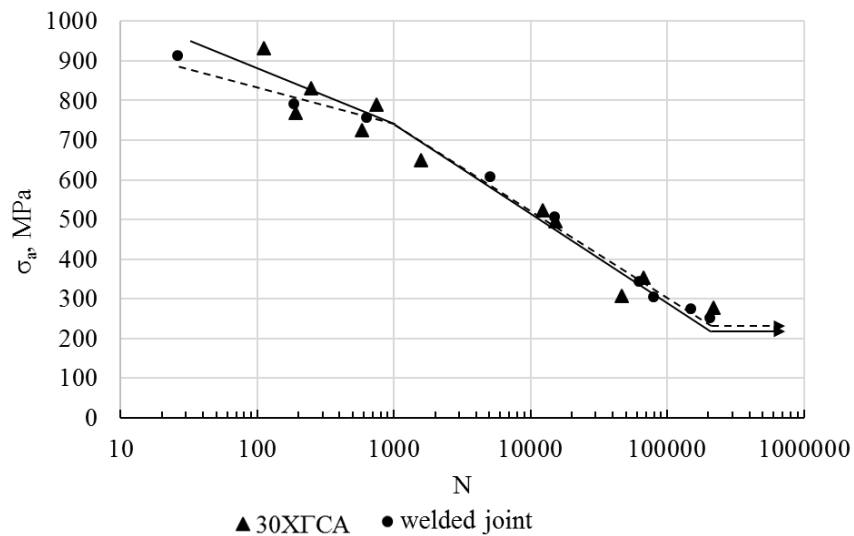


Fig. 8. Limited endurance curves of the 30XГСА steel and a welded joint of 30XГСА–40XMΦA steels
Рис. 8. Кривые ограниченной выносливости стали 30XГСА и сварного соединения сталей 30XГСА–40XMΦA

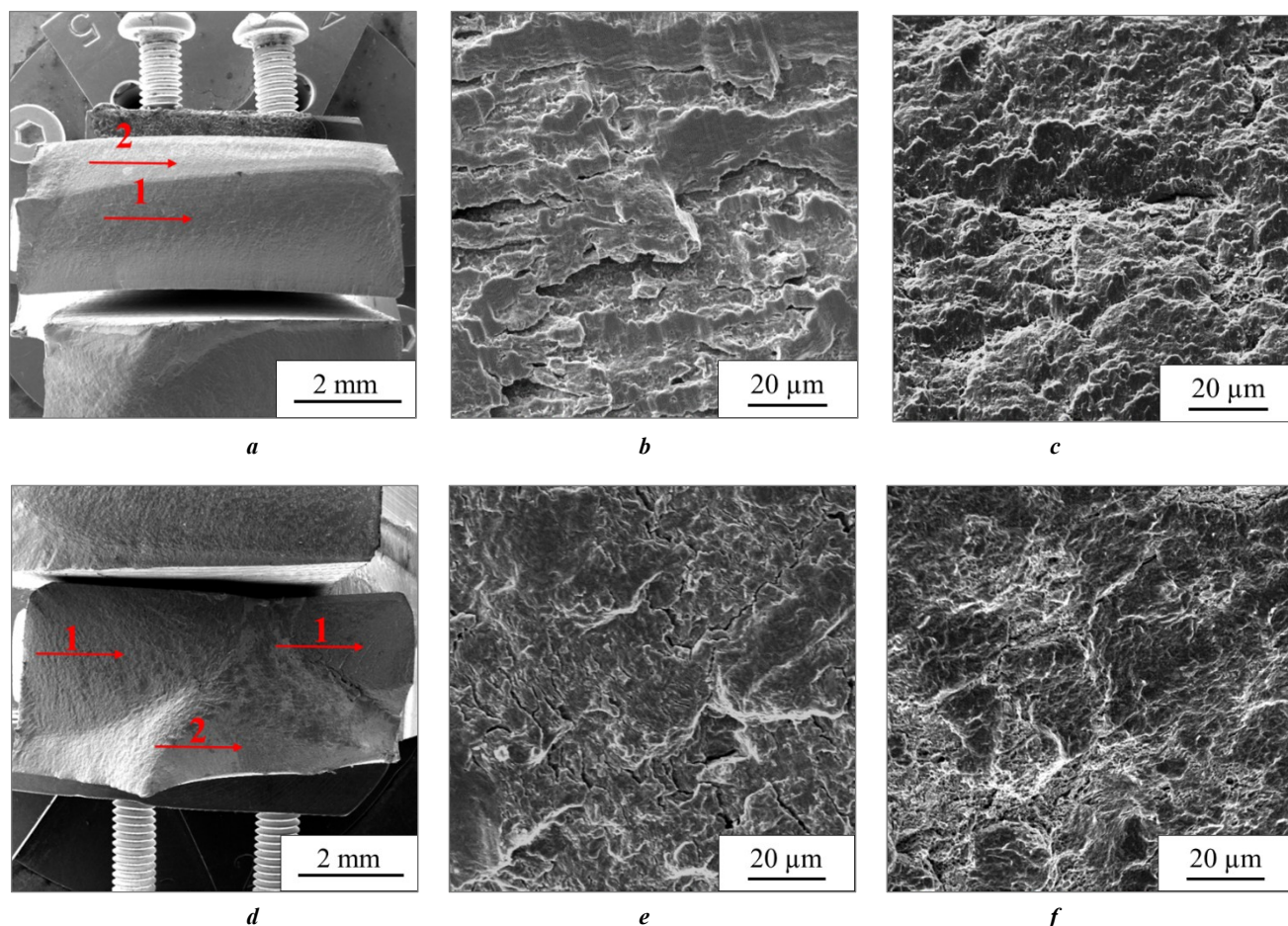


Fig. 9. Macro- (a, d) and microstructure (b, c, e, f) of fractures of a 30XГСА–40ХМФА welded joint ($\sigma_a=495$ MPa, $N=15077$) (a–c) and a monolithic specimen of the 30XГСА steel ($\sigma_a=508$ MPa, $N=14965$) (d–f) obtained at low-cycle fatigue tests:

a, d – general appearance; b, e – area 1 (fatigue zone); c, f – area 2 (fracture zone)

Рис. 9. Макро- (a, d) и микростроение (b, c, e, f) изломов сварного соединения 30XГСА–40ХМФА ($\sigma_a=495$ МПа, $N=15077$) (a–c) и монолитного образца стали 30XГСА ($\sigma_a=508$ МПа, $N=14965$) (d–f), полученных при испытаниях в условиях малоциклового усталости:

a, d – общий вид; b, e – участок 1 (зона усталости); c, f – участок 2 (зона долома)

of various factors accompanying fracture. Despite this, the fatigue fracture is well identified in all samples when studying the propagation of the direction of secondary cracks perpendicular to the main crack. Secondary cracks are more clearly expressed in the sample with a welded joint (Fig. 10 b) compared to the base metal. Most probably, this occurs due to the formation of a crystallographic texture in the welded joint zone under the influence of the thermal deformation cycle of welding [24]. The fracture zones of both samples (Fig. 10 c, 10 f) have a typical shallow-pitted relief.

DISCUSSION

The results of the study showed that the welded joint of 30XГСА and 40ХМФА steels under certain welding parameters is capable of ensuring a full-strength structure with the 30XГСА steel both under the static tension, as established in the work [25], and under cyclic loading. One of the RFW parameters affecting the properties of a welded joint is the force during heating. The present study identified that with an increase in the force during heating, the TME zones strengthen at the reduction in their length

from the side of each type of steel, which contributes to an increase in the fatigue endurance of the studied welded joints. Most probably, this effect is caused by the intensification of the processes of strain hardening in the TME zones implemented during RFW, as established in the work [12]. However, when the deformed microstructure is heated, the recovery and polygonization processes develop, which are accompanied by local softening of the materials in the TMEZ and a decrease in fatigue endurance, which was also observed in the work [26]. The fatigue crack growth rate increases, which is confirmed by the results of microfractographic analysis. Therefore, tempering of a welded joint of 30XГСА–40ХМФА steels will have a negative impact on the properties of the structure.

MAIN RESULTS AND CONCLUSIONS

1. The study identified that with an increase in the force during heating in the process of RFW of tubular billets of the H standard size according to ISO 10097 made of 30XГСА and 40ХМФА steels in the range from 40 to 120 kN, microstructural changes occur, accompanied by

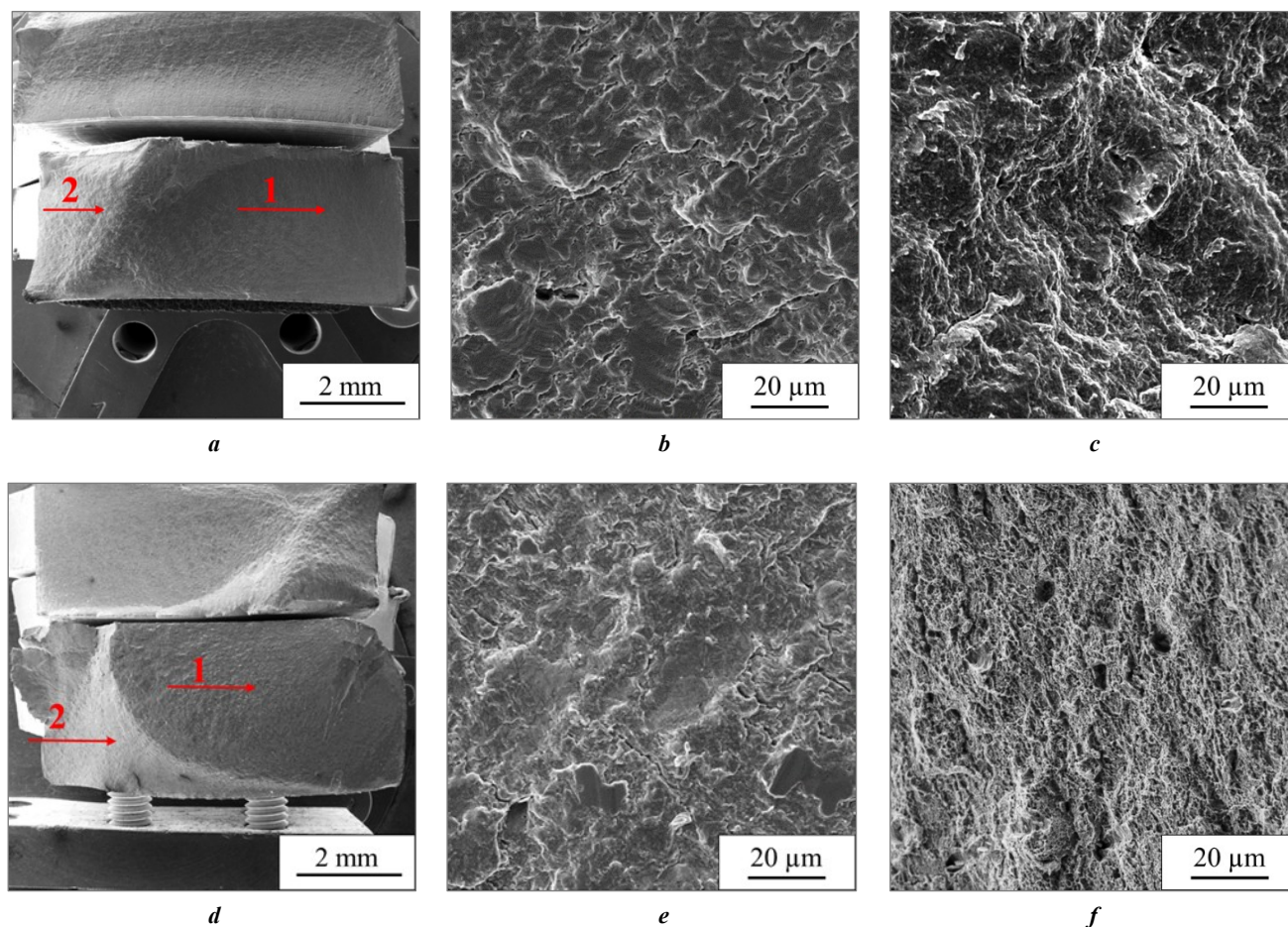


Fig. 10. Macro- (a, d) and microstructure (b, c, e, f) of fractures of 30XГСА–40XMΦA welded joints ($\sigma_a=354$ MPa, $N=67321$) (a–c) and a monolithic specimen of the 30XГСА steel ($\sigma=342$ MPa, $N=62400$) (d–f) obtained at multicycle fatigue tests:

a, d – general appearance; b, e – area 1 (fatigue zone); c, f – area 2 (fracture zone)

Рис. 10. Макро- (a, d) и микростроение (b, c, e, f) изломов сварных соединений 30XГСА–40XMΦA ($\sigma_a=354$ МПа, $N=67321$) (a–c) и монолитного образца стали 30XГСА ($\sigma=342$ МПа, $N=62400$) (d–f), полученных при испытаниях в условиях многоциклового усталости:
a, d – общий вид; b, e – участок 1 (зона усталости); c, f – участок 2 (зона долома)

a reduction in the TMEZ length and strengthening of the peripheral areas, which contributes to an increase in the fatigue strength of welded joints.

2. Post-weld tempering causes a decrease in the number of cycles before failure compared to the initial state of welded joints by 15–40 %, depending on the welding mode. In this case, tempering leads to the formation of a smoother microrelief in the fracture and an increase in the distance between the fatigue failure grooves.

3. Based on the research, the optimal RFW mode was determined for the lightened structures of the H standard size exploration drill pipes, which corresponds to the force during heating (at friction) $F_n=120$ kN, the forging force $F_{for}=160$ kN, the rotational speed during heating $n=800$ Rpm, and the upset during heating $l=8$ mm. With the specified RFW process parameters, the fatigue strength of welded joints is comparable to the fatigue strength of the base metal of the weakest 30XГСА steel, which is confirmed by the limited endurance curves and the almost identical nature of the destruction revealed by macro- and microfractographic studies.

REFERENCES

1. Emre H.E., Kaçar R. Effect of Post Weld Heat Treatment Process on Microstructure and Mechanical Properties of Friction Welded Dissimilar Drill Pipe. *Materials Research*, 2015, vol. 18, no. 3, pp. 503–508. DOI: [10.1590/1516-1439.308114](https://doi.org/10.1590/1516-1439.308114).
2. Banerjee A., Ntovas M., Da Silva L., Rahimi S., Wynne B. Inter-relationship between microstructure evolution and mechanical properties in inertia friction welded 8630 low-alloy steel. *Archives of Civil and Mechanical Engineering*, 2021, vol. 21, article number 149. DOI: [10.1007/s43452-021-00300-9](https://doi.org/10.1007/s43452-021-00300-9).
3. Khadeer Sk.A., Babu P.R., Kumar B.R., Kumar A.S. Evaluation of friction welded dissimilar pipe joints between AISI 4140 and ASTM A 106 Grade B steels used in deep exploration drilling. *Journal of Manufacturing Processes*, 2020, vol. 56, pp. 197–205. DOI: [10.1016/j.jmapro.2020.04.078](https://doi.org/10.1016/j.jmapro.2020.04.078).
4. Kumar A.S., Khadeer Sk.A., Rajinikanth V., Pahari S., Kumar B.R. Evaluation of bond interface characteristics of rotary friction welded carbon steel to low alloy steel pipe joints. *Materials Science & Engineering A*, 2021,

- vol. 824, article number 141844. DOI: [10.1016/j.msea.2021.141844](https://doi.org/10.1016/j.msea.2021.141844).
5. Li P., Wang S., Xia Y., Hao X., Lei Z., Dong H. Inhomogeneous microstructure and mechanical properties of rotary friction welded AA2024 joints. *Journal of Materials Research and Technology*, 2020, vol. 9, no. 3, pp. 5749–5760. DOI: [10.1016/j.jmrt.2020.03.100](https://doi.org/10.1016/j.jmrt.2020.03.100).
 6. Nagaraj M., Ravisankar B. Effect of Severe Plastic Deformation on Microstructure and Mechanical Behaviour of Friction-Welded Structural Steel IS2062. *Transactions of the Indian Institute of Metals*, 2019, vol. 72, pp. 751–756. DOI: [10.1007/s12666-018-1527-1](https://doi.org/10.1007/s12666-018-1527-1).
 7. Jeffrey W.S., Thomas G.H., McColskey J.D., Victor F.P., Ramirez A.J. Characterization of mechanical properties, fatigue-crack propagation, and residual stresses in a microalloyed pipeline-steel friction-stir weld. *Materials and Design*, 2015, vol. 88, pp. 632–642. DOI: [10.1016/j.matdes.2015.09.049](https://doi.org/10.1016/j.matdes.2015.09.049).
 8. Abdulstaar M.A., Al-Fadhlah K.J., Wagner L. Microstructural variation through weld thickness and mechanical properties of peened friction stir welded 6061 aluminum alloy joints. *Materials Characterization*, 2017, vol. 126, pp. 64–73. DOI: [10.1016/j.matchar.2017.02.011](https://doi.org/10.1016/j.matchar.2017.02.011).
 9. Mc Pherson N.A., Galloway A.M., Cater S.R., Hambling S.J. Friction stir welding of thin DH36 steel plate. *Science and Technology of Welding & Joining*, 2013, vol. 18, pp. 441–450. DOI: [10.1179/1362171813Y.0000000122](https://doi.org/10.1179/1362171813Y.0000000122).
 10. Baillie P., Campbell S., Galloway A., Cater S.R., Mcpherson N.A. A Comparison of Double Sided Friction Stir Welding in Air and Underwater for 6mm S275 Steel Plate. *International Journal of Chemical, Nuclear, Metallurgical and Materials Engineering*, 2014, vol. 8, pp. 651–655. DOI: [10.13140/2.1.2306.2400](https://doi.org/10.13140/2.1.2306.2400).
 11. Ericsson M., Sandstrom R. Influence of welding speed on the fatigue of friction stir welds, and comparison with MIG and TIG. *International Journal of Fatigue*, 2003, vol. 25, no. 12, pp. 1379–1387. DOI: [10.1016/S0142-1123\(03\)00059-8](https://doi.org/10.1016/S0142-1123(03)00059-8).
 12. Yamamoto Y., Ochi H., Sawai T., Ogawa K., Tsujino R., Yasutomi M. Tensile Strength and Fatigue Strength of Friction-Welded SUS304 Stainless Steel Joints-Evaluation of Joint Strength by Deformation Heat Input in Upset Stage and Upset Burn-Off Length. *Journal of the Society of Materials Science Japan*, 2004, vol. 53, no. 5, pp. 512–517. DOI: [10.2472/jsms.53.5.12](https://doi.org/10.2472/jsms.53.5.12).
 13. Paventhan R., Lakshminarayanan P.R., Balasubramanian V. Fatigue behaviour of friction welded medium carbon steel and austenitic stainless steel dissimilar joints. *Materials and Design*, 2011, vol. 32, no. 4, pp. 1888–1894. DOI: [10.1016/j.matdes.2010.12.011](https://doi.org/10.1016/j.matdes.2010.12.011).
 14. Sahin M. Joining with friction welding of high speed and medium carbon steel. *Journal of Materials Processing Technology*, 2005, vol. 168, no. 2, pp. 168–202. DOI: [10.1016/j.jmatprotec.2004.11.015](https://doi.org/10.1016/j.jmatprotec.2004.11.015).
 15. Atamashkin A.S., Priymak E.Yu., Tulibaev E.S., Stepanchukova A.V. Endurance limit and mechanism of fracture of friction welded joints of exploration drill pipes in the conditions of multi-cycle fatigue. *Chernye metally*, 2021, no. 5, pp. 33–38. DOI: [10.17580/chm.2021.05.06](https://doi.org/10.17580/chm.2021.05.06).
 16. Belkahla Y., Mazouzi A., Lebouachera S.E.I., Hassan A.J., Fides M., Hvizdoš P., Cheniti B., Miroud D. Rotary friction welded C45 to 16NiCr6 steel rods: statistical optimization coupled to mechanical and microstructure approaches. *The International Journal of Advanced Manufacturing Technology*, 2021, vol. 116, pp. 2285–2298. DOI: [10.1007/s00170-021-07597-z](https://doi.org/10.1007/s00170-021-07597-z).
 17. Selvamani S.T., Vigneshwar M., Nikhil M., Hariharan S.J., Palanikumar K. Enhancing the Fatigue Properties of Friction Welded AISI 1020 Grade Steel Joints using Post Weld Heat Treatment Process in Optimized Condition. *Materials Today: Proceedings*, 2019, vol. 16-2, pp. 1251–1258. DOI: [10.1016/j.matpr.2019.05.222](https://doi.org/10.1016/j.matpr.2019.05.222).
 18. Mercan S., Aydin S., Özdemir N. Effect of welding parameters on the fatigue properties of dissimilar AISI 2205–AISI 1020 joined by friction welding. *International Journal of Fatigue*, 2015, vol. 81, pp. 78–90. DOI: [10.1016/j.ijfatigue.2015.07.023](https://doi.org/10.1016/j.ijfatigue.2015.07.023).
 19. Barrionuevo G.O., Mullo J.L., Ramos-Grez J.A. Predicting the ultimate tensile strength of AISI 1045 steel and 2017-T4 aluminum alloy joints in a laser-assisted rotary friction welding process using machine learning: a comparison with response surface methodology. *The International Journal of Advanced Manufacturing Technology*, 2021, vol. 116, pp. 1247–1257. DOI: [10.1007/s00170-021-07469-6](https://doi.org/10.1007/s00170-021-07469-6).
 20. Lukin V.I., Ovsepyan S.V., Kovalchuk V.G., Samorukov M.L. Features of rotary friction welding of high-temperature nickel alloy VZh175. *Trudy VIAM*, 2017, no. 12, pp. 3–12. DOI: [10.18577/2307-6046-2017-0-12-1-1](https://doi.org/10.18577/2307-6046-2017-0-12-1-1).
 21. Fang Y., Jiang X., Mo D., Zhu D., Luo Z. A review on dissimilar metals' welding methods and mechanisms with interlayer. *The International Journal of Advanced Manufacturing Technology*, 2019, vol. 102, pp. 2845–2863. DOI: [10.1007/s00170-019-03353-6](https://doi.org/10.1007/s00170-019-03353-6).
 22. Kuzmina E.A., Priymak E.Yu., Kirilenko A.S. Optimization of parameters of friction stir welded unlike joints of medium-carbon alloy steels 30KhGSA and 40KhMFA. *Metal Science and Heat Treatment*, 2023, vol. 64, no. 9-10, pp. 596–602. DOI: [10.1007/s11041-023-00855-9](https://doi.org/10.1007/s11041-023-00855-9).
 23. Vill V.I. *Svarka metallov treniem* [Friction welding of metals]. Moscow, Mashinostroenie Publ., 1970. 176 p.
 24. Priymak E.Yu., Lobanov M.L., Belikov S.V., Karabanalov M.S., Yakovleva I.L. Structure Formation Patterns and Crystallographic Texture in Welded Joints of Medium-Carbon Alloy Steels in the Process of Rotary Friction Welding. *Physics of Metals and Metallography*, 2022, vol. 123, no. 6, pp. 559–566. DOI: [10.1134/S0031918X22060126](https://doi.org/10.1134/S0031918X22060126).
 25. Kuzmina E.A., Priymak E.Yu., Kirilenko A.S., Semka Ya.S. Influence of the heating force in rotational friction welding on mechanical properties and tensile fracture mechanism of dissimilar welded joints of 30KhGSA and 40KhMFA steels. *Chernye metally*, 2022, no. 12, pp. 49–57. DOI: [10.17580/chm.2022.12.07](https://doi.org/10.17580/chm.2022.12.07).
 26. Atamashkin A.S., Priymak E.Yu. The influence of postweld tempering on mechanical behavior of friction welded joints of 32G2 and 40HN steels under high-cycle fatigue. *Vektor nauki Tolyattinskogo gosudarstvennogo universiteta*, 2021, no. 3, pp. 7–18. DOI: [10.18323/2073-5073-2021-3-7-18](https://doi.org/10.18323/2073-5073-2021-3-7-18).

СПИСОК ЛІТЕРАТУРИ

1. Emre H.E., Kaçar R. Effect of Post Weld Heat Treatment Process on Microstructure and Mechanical Properties of Friction Welded Dissimilar Drill Pipe // *Materials*

- Research. 2015. Vol. 18. № 3. P. 503–508. DOI: [10.1590/1516-1439.308114](https://doi.org/10.1590/1516-1439.308114).
2. Banerjee A., Ntovas M., Da Silva L., Rahimi S., Wynne B. Inter-relationship between microstructure evolution and mechanical properties in inertia friction welded 8630 low-alloy steel // Archives of Civil and Mechanical Engineering. 2021. Vol. 21. Article number 149. DOI: [10.1007/s43452-021-00300-9](https://doi.org/10.1007/s43452-021-00300-9).
 3. Khadeer Sk.A., Babu P.R., Kumar B.R., Kumar A.S. Evaluation of friction welded dissimilar pipe joints between AISI 4140 and ASTM A 106 Grade B steels used in deep exploration drilling // Journal of Manufacturing Processes. 2020. Vol. 56. P. 197–205. DOI: [10.1016/j.jmapro.2020.04.078](https://doi.org/10.1016/j.jmapro.2020.04.078).
 4. Kumar A.S., Khadeer Sk.A., Rajinikanth V., Pahari S., Kumar B.R. Evaluation of bond interface characteristics of rotary friction welded carbon steel to low alloy steel pipe joints // Materials Science & Engineering A. 2021. Vol. 824. Article number 141844. DOI: [10.1016/j.msea.2021.141844](https://doi.org/10.1016/j.msea.2021.141844).
 5. Li P., Wang S., Xia Y., Hao X., Lei Z., Dong H. Inhomogeneous microstructure and mechanical properties of rotary friction welded AA2024 joints // Journal of Materials Research and Technology. 2020. Vol. 9. № 3. P. 5749–5760. DOI: [10.1016/j.jmrt.2020.03.100](https://doi.org/10.1016/j.jmrt.2020.03.100).
 6. Nagaraj M., Ravisankar B. Effect of Severe Plastic Deformation on Microstructure and Mechanical Behaviour of Friction-Welded Structural Steel IS2062 // Transactions of the Indian Institute of Metals. 2019. Vol. 72. P. 751–756. DOI: [10.1007/s12666-018-1527-1](https://doi.org/10.1007/s12666-018-1527-1).
 7. Jeffrey W.S., Thomas G.H., McColskey J.D., Victor F.P., Ramirez A.J. Characterization of mechanical properties, fatigue-crack propagation, and residual stresses in a microalloyed pipeline-steel friction-stir weld // Materials and Design. 2015. Vol. 88. P. 632–642. DOI: [10.1016/j.matdes.2015.09.049](https://doi.org/10.1016/j.matdes.2015.09.049).
 8. Abdulstaar M.A., Al-Fadhlah K.J., Wagner L. Microstructural variation through weld thickness and mechanical properties of peened friction stir welded 6061 aluminum alloy joints // Materials Characterization. 2017. Vol. 126. P. 64–73. DOI: [10.1016/j.matchar.2017.02.011](https://doi.org/10.1016/j.matchar.2017.02.011).
 9. Mc Pherson N.A., Galloway A.M., Cater S.R., Hambling S.J. Friction stir welding of thin DH36 steel plate // Science and Technology of Welding & Joining. 2013. Vol. 18. P. 441–450. DOI: [10.1179/1362171813Y.0000000122](https://doi.org/10.1179/1362171813Y.0000000122).
 10. Baillie P., Campbell S., Galloway A., Cater S.R., Mcpherson N.A. A Comparison of Double Sided Friction Stir Welding in Air and Underwater for 6mm S275 Steel Plate // International Journal of Chemical, Nuclear, Metallurgical and Materials Engineering. 2014. Vol. 8. P. 651–655. DOI: [10.13140/2.1.2306.2400](https://doi.org/10.13140/2.1.2306.2400).
 11. Ericsson M., Sandstrom R. Influence of welding speed on the fatigue of friction stir welds, and comparison with MIG and TIG // International Journal of Fatigue. 2003. Vol. 25. № 12. P. 1379–1387. DOI: [10.1016/S0142-1123\(03\)00059-8](https://doi.org/10.1016/S0142-1123(03)00059-8).
 12. Yamamoto Y., Ochi H., Sawai T., Ogawa K., Tsujino R., Yasutomi M. Tensile Strength and Fatigue Strength of Friction-Welded SUS304 Stainless Steel Joints-Evaluation of Joint Strength by Deformation Heat Input in Upset Stage and Upset Burn-Off Length // Journal of the Society of Materials Science Japan. 2004. Vol. 53. № 5. P. 512–517. DOI: [10.2472/jsms.53.512](https://doi.org/10.2472/jsms.53.512).
 13. Paventhan R., Lakshminarayanan P.R., Balasubramanian V. Fatigue behaviour of friction welded medium carbon steel and austenitic stainless steel dissimilar joints // Materials and Design. 2011. Vol. 32. № 4. P. 1888–1894. DOI: [10.1016/j.matdes.2010.12.011](https://doi.org/10.1016/j.matdes.2010.12.011).
 14. Sahin M. Joining with friction welding of high speed and medium carbon steel // Journal of Materials Processing Technology. 2005. Vol. 168. № 2. P. 168–202. DOI: [10.1016/j.jmatprotec.2004.11.015](https://doi.org/10.1016/j.jmatprotec.2004.11.015).
 15. Атамашкин А.С., Приймак Е.Ю., Тулибаев Е.С., Степанчукова А.В. Предел выносливости и механизм разрушения фрикционных сварных соединений геолого-разведочных буровых труб // Черные металлы. 2021. № 5. С. 33–38. DOI: [10.17580/chm.2021.05.06](https://doi.org/10.17580/chm.2021.05.06).
 16. Belkahla Y., Mazouzi A., Lebouachera S.E.I., Hassan A.J., Fides M., Hvizdoš P., Cheniti B., Miroud D. Rotary friction welded C45 to 16NiCr6 steel rods: statistical optimization coupled to mechanical and microstructure approaches // The International Journal of Advanced Manufacturing Technology. 2021. Vol. 116. P. 2285–2298. DOI: [10.1007/s00170-021-07597-z](https://doi.org/10.1007/s00170-021-07597-z).
 17. Selvamani S.T., Vigneshwar M., Nikhil M., Hariharan S.J., Palanikumar K. Enhancing the Fatigue Properties of Friction Welded AISI 1020 Grade Steel Joints using Post Weld Heat Treatment Process in Optimized Condition // Materials Today: Proceedings. 2019. Vol. 16-2. P. 1251–1258. DOI: [10.1016/j.matpr.2019.05.222](https://doi.org/10.1016/j.matpr.2019.05.222).
 18. Mercan S., Aydin S., Özdemir N. Effect of welding parameters on the fatigue properties of dissimilar AISI 2205–AISI 1020 joined by friction welding // International Journal of Fatigue. 2015. Vol. 81. P. 78–90. DOI: [10.1016/j.ijfatigue.2015.07.023](https://doi.org/10.1016/j.ijfatigue.2015.07.023).
 19. Barrionuevo G.O., Mullo J.L., Ramos-Grez J.A. Predicting the ultimate tensile strength of AISI 1045 steel and 2017-T4 aluminum alloy joints in a laser-assisted rotary friction welding process using machine learning: a comparison with response surface methodology // The International Journal of Advanced Manufacturing Technology. 2021. Vol. 116. P. 1247–1257. DOI: [10.1007/s00170-021-07469-6](https://doi.org/10.1007/s00170-021-07469-6).
 20. Лукин В.И., Овсепян С.В., Ковальчук В.Г., Саморук М.Л. Особенности ротационной сварки трением высокожаропрочного никелевого сплава ВЖ175 // Труды ВИАМ. 2017. № 12. С. 3–12. DOI: [10.18577/2307-6046-2017-0-12-1-1](https://doi.org/10.18577/2307-6046-2017-0-12-1-1).
 21. Fang Y., Jiang X., Mo D., Zhu D., Luo Z. A review on dissimilar metals' welding methods and mechanisms with interlayer // The International Journal of Advanced Manufacturing Technology. 2019. Vol. 102. P. 2845–2863. DOI: [10.1007/s00170-019-03353-6](https://doi.org/10.1007/s00170-019-03353-6).
 22. Кузьмина Е.А., Приймак Е.Ю., Кириленко А.С. Оптимизация параметров ротационной сварки трением разнородных сварных соединений среднеуглеродистых легированных сталей 30ХГСА и 40ХМФА // Металловедение и термическая обработка металлов. 2022. № 10. С. 52–59. DOI: [10.30906/mitom.2022.10.52-59](https://doi.org/10.30906/mitom.2022.10.52-59).
 23. Вилль В.И. Сварка металлов трением. М.: Машиностроение, 1970. 176 с.
 24. Priymak E.Yu., Lobanov M.L., Belikov S.V., Karabanalov M.S., Yakovleva I.L. Structure Formation Patterns and Crystallographic Texture in Welded Joints of Medium-Carbon Alloy Steels in the Process of Rotary Friction Welding // Physics of Metals and Metallo-

- graphy. 2022. Vol. 123. № 6. P. 559–566. DOI: [10.1134/S0031918X22060126](https://doi.org/10.1134/S0031918X22060126).
25. Кузьмина Е.А., Приймак Е.Ю., Кириленко А.С., Сёмка Я.С. Влияние силы нагрева при ротационной сварке трением на механические свойства и механизм разрушения при растяжении разнородных сварных соединений сталей 30ХГСА и 40ХМФА // Черные металлы. 2022. № 12. С. 49–57. DOI: [10.17580/chm.2022.12.07](https://doi.org/10.17580/chm.2022.12.07).
26. Атамашкин А.С., Приймак Е.Ю. Влияние послесварочного отпуска на механическое поведение трещинообразующих сварных соединений сталей 32Г2 и 40ХН в условиях многоциклового усталости // Вектор науки Тольяттинского государственного университета. 2021. № 3. С. 7–18. DOI: [10.18323/2073-5073-2021-3-7-18](https://doi.org/10.18323/2073-5073-2021-3-7-18).

Усталостная прочность сварных соединений сталей 30ХГСА–40ХМФА, полученных ротационной сваркой трением

© 2023

Приймак Елена Юрьевна^{*1,2,4}, кандидат технических наук, заведующий лабораторией металловедения и термической обработки, доцент кафедры материаловедения и технологии материалов
Кузьмина Елена Александровна¹, начальник технического отдела
Гладковский Сергей Викторович^{3,5}, доктор технических наук, главный научный сотрудник
Вичужанин Дмитрий Иванович^{3,6}, кандидат технических наук, старший научный сотрудник
Веселова Валерия Евгеньевна^{3,7}, младший научный сотрудник

¹АО «Завод бурового оборудования», Оренбург (Россия)

²Оренбургский государственный университет, Оренбург (Россия)

³Институт машиноведения имени Э.С. Горкунова УрО РАН, Екатеринбург (Россия)

*E-mail: elena-pijmak@yandex.ru

⁴ORCID: <https://orcid.org/0000-0002-4571-2410>

⁵ORCID: <https://orcid.org/0000-0002-3542-6242>

⁶ORCID: <https://orcid.org/0000-0002-6508-6859>

⁷ORCID: <https://orcid.org/0000-0002-4955-6435>

Поступила в редакцию 02.11.2022

Принята к публикации 16.02.2023

Аннотация: Ротационная сварка трением (РСТ) используется при производстве бурильных труб для геолого-разведки на твердые полезные ископаемые. Потребность в создании облегченных колонн бурильных труб для высокоскоростного алмазного бурения сверхглубоких скважин диктует необходимость более пристального внимания к изучению зоны сварного шва и назначению технологических параметров РСТ. В работе приведены результаты экспериментальных исследований сварного соединения бурильной трубы типоразмера H по ISO 10097 из сталей 30ХГСА (тело трубы) и 40ХМФА (замковая часть) в условиях воздействия циклических нагрузок. Оценивалось влияние силы, прикладываемой к заготовкам в процессе трения соприкасающихся поверхностей (силы при нагреве), и послесварочного отпуска при температуре 550 °С на циклическую долговечность сварных соединений в условиях знакопеременного растяжения-сжатия при напряжении амплитуды цикла ± 420 МПа. Установлено, что с увеличением силы при нагреве в зоне термомеханического влияния происходят изменения микроструктуры, способствующие повышению усталостной прочности сварных соединений. Выявлено негативное влияние послесварочного отпуска на усталостную прочность сварных соединений, выражающееся в снижении количества циклов до разрушения на 15–40 % в зависимости от величины силы при нагреве. Определен оптимальный режим РСТ указанного сочетания сталей, обеспечивающий наибольшее количество циклов до разрушения: сила при нагреве (при трении) $F_H=120$ кН, сила проковки $F_{пр}=160$ кН, частота вращения при нагреве $n=800$ об/мин и осадка при нагреве $l=8$ мм. Проведена серия усталостных испытаний при различных значениях напряжения амплитуды цикла сварного соединения, полученного на оптимальном режиме, и основного металла стали 30ХГСА; построены кривые ограниченной выносливости. Показано, что различия в кривых ограниченной выносливости материала тела трубы (сталь 30ХГСА) и сварного соединения незначительны. Полученные результаты дополнены данными измерений микротвердости и фрактограммами разрушенных образцов, раскрывающими механизм распространения трещин в условиях воздействия циклических нагрузок.

Ключевые слова: ротационная сварка трением; бурильные трубы; сварное соединение; усталостная прочность; кривая ограниченной выносливости; сталь 30ХГСА; сталь 40ХМФА.

Благодарности: Исследование выполнено при финансовой поддержке РФФИ в рамках научного проекта № 20-38-90032.

При проведении механических испытаний использовалось оборудование, входящее в состав ЦКП «Пластометрия» Института машиноведения имени Э.С. Горкунова УрО РАН.

Для цитирования: Приймак Е.Ю., Кузьмина Е.А., Гладковский С.В., Вичужанин Д.И., Веселова В.Е. Усталостная прочность сварных соединений сталей 30ХГСА–40ХМФА, полученных ротационной сваркой трением // Frontier Materials & Technologies. 2023. № 1. С. 69–81. DOI: [10.18323/2782-4039-2023-1-69-81](https://doi.org/10.18323/2782-4039-2023-1-69-81).